

Effectiveness of mixing in violent relaxationPierre de Buyl^{1,2} and Pierre Gaspard¹¹*Center for Nonlinear Phenomena and Complex Systems, Université Libre de Bruxelles, Code Postal 231, Campus Plaine, BE-1050 Brussels, Belgium*²*Chemical Physics Theory Group, Department of Chemistry, University of Toronto, Toronto, Ontario M5S 3H6, Canada*

(Received 2 August 2011; revised manuscript received 23 November 2011; published 22 December 2011)

Relaxation processes in collisionless dynamics lead to peculiar behavior in systems with long-range interactions such as self-gravitating systems, non-neutral plasmas, and wave-particle systems. These systems, adequately described by the Vlasov equation, present quasistationary states (QSS), i.e., long lasting intermediate stages of the dynamics that occur after a short significant evolution called “violent relaxation.” The nature of the relaxation, in the absence of collisions, is not yet fully understood. We demonstrate in this article the occurrence of stretching and folding behavior in numerical simulations of the Vlasov equation, providing a plausible relaxation mechanism that brings the system from its initial condition into the QSS regime. Area-preserving discrete-time maps with a mean-field coupling term are found to display a similar behavior in phase space as the Vlasov system.

DOI: [10.1103/PhysRevE.84.061139](https://doi.org/10.1103/PhysRevE.84.061139)

PACS number(s): 05.20.-y, 05.45.-a, 05.10.-a, 52.20.-j

I. INTRODUCTION

The evolution of collisionless systems poses an interesting challenge in kinetic theory. Indeed, from the lack of a collision term in the kinetic equation ruling the evolution of the system arises the need for another relaxation mechanism. Unusual relaxation properties are found in many physical systems, among which are self-gravitating systems, non-neutral plasmas, and wave-particle interactions. These systems fall into the categories of long-range interacting systems, a domain of physics that is the object of renewed interest [1–3].

One phenomenon in particular has been evidenced numerically [4] and theoretically [5,6]: In systems with long-range interactions, increasing the number of particles N causes the system to evolve, with a time scale of order N^0 , toward an intermediate state that is not the one predicted by statistical mechanics and whose lifetime increases as N^δ , with $\delta \geq 1/8$ [7]. Numerical simulations show algebraic increase with $\delta \simeq 1$ [8] or $\delta \simeq 1.7$ [4] depending on the conditions. These long lasting intermediate states are called quasistationary states (QSS) and are equilibria of the continuum limit given by the Vlasov equation [4]. QSS have been observed in the Hamiltonian mean-field (HMF) model [9], the free-electron laser [10], and also in self-gravitating systems [11]. Experimental perspectives regarding these QSS have recently been proposed [12].

The fast evolution on a timescale N^0 is termed violent relaxation, following the terminology of the studies on one-dimensional self-gravitating systems. Early works report that the evolution toward a stationary regime is not driven by two-body encounters and question the nature of the initial evolution of gravitating systems [13,14]. In light of these observations, Lynden-Bell presented in 1967 his *statistical mechanics of violent relaxation in stellar systems* [15]. The aim of his theory is to explain the outcome of collisionless dynamics and the unusual energy distribution found in galactic dynamics. Lynden-Bell’s (LB) theory is a statistical theory that takes into account, among other properties of the Vlasov equation, its incompressible character in the single-particle phase space; accordingly, an ergodic-type hypothesis on the dynamics allows one to compute, via an entropy maximization,

stationary states of the Vlasov equation. LB’s theory predicts the magnetization in the HMF model and provides the most likely QSS solution for this model, as of now [16,17]. The work of Lynden-Bell has been followed by numerous numerical studies on violent relaxation; see Refs. [18–21] for instance. LB’s theory or other attempts to compute the outcome of violent relaxation can be found in more recent work on the self-gravitating sheet model [11], non-neutral plasmas [22], and two-dimensional (2D) self-gravitating systems [23]. Recently, new macroscopic observables have been proposed to measure the approach to equilibrium in the self-gravitating sheet model [24]. An extensive study by the same authors indicates the physical situations in which LB’s theory provides a good prediction and the reasons it does not work in other situations [25].

Let us also mention the use of the Vlasov equation in the field of plasma physics [26], that is probably the widest area of research making use of it. The understanding of collisionless relaxation is also of great interest in this field and is mostly known for the famous problem of Landau damping (see Ref. [27] for instance).

The purpose of this article is to demonstrate via direct numerical simulation of the Vlasov equation that stretching and folding structures occur in some regions of phase space. A measure of the consequent deformation of the fluid allows us to characterize the short-time evolution in the Vlasov equation. We thus suggest that the stretching and folding mechanism is a collisionless source of mixing evolution toward the QSS, the mechanism from which the violent relaxation originates. We choose to take as the main vehicle of our study the Hamiltonian mean-field (HMF) model [28], a system of globally coupled rotators moving on a circle. The HMF model has been the object of many studies as a paradigmatic representative of long-range interacting systems, and the properties of its associated Vlasov dynamics are well known. In addition, in the spirit of demonstrating fundamental dynamical properties, the similarity of the HMF model with the forced pendulum makes it a worthwhile example, as evidenced in Ref. [29].

We also consider discrete-time versions of Vlasov dynamics, in which the phase-space distribution function evolves

under the effect of an area-preserving map. Two such mean-field maps are investigated, which are based on Arnold's cat map [30,31] and the standard map [32,33].

The plan of the paper is the following. In Sec. II, we introduce the Hamiltonian mean-field model, its associated Vlasov equation, and the phenomenology of QSS. Section III presents the numerical algorithm and the computation of the perimeter that is used to substantiate quantitatively our claims. Section IV gives the results of Vlasov simulations, in which stretching and folding occur in phase space. In Sec. V, mean-field maps are studied in order to determine the conditions of stretching of fluid boundaries in phase space.

II. COLLISIONLESS DYNAMICS AND THE HAMILTONIAN MEAN-FIELD MODEL

The Hamiltonian mean-field (HMF) model was introduced as a simplified model to study collective effects and has become a paradigmatic model to study long-range interactions [3,28]. It is composed of particles on a circle interacting via a cosine potential and described by the following Hamiltonian:

$$H = \sum_{i=1}^N \frac{p_i^2}{2} + \frac{1}{2N} \sum_{i,j=1}^N [1 - \cos(\theta_i - \theta_j)], \quad (1)$$

where θ_i is the position in the interval $[-\pi; \pi[$ of the i th particle, p_i is its momentum, and N is the number of particles. At equilibrium, the HMF model is characterized by a second-order phase transition, identified by the magnetization:

$$\mathbf{m} = m_x + i m_y = \frac{1}{N} \sum_{j=1}^N e^{i\theta_j}. \quad (2)$$

$m = |\mathbf{m}|$ is equal to zero above the critical energy $u_c = \frac{H}{N} = \frac{3}{4}$, while $m > 0$ for energies below u_c .

Starting from an out-of-equilibrium initial condition, the HMF model displays interesting dynamical phenomena: in addition to the energy, the initial value of m influences the regimes attained by the system [17], a dependence which is not found at equilibrium. The value that m reaches is not the one corresponding to equilibrium statistical mechanics. This phenomenon lasts for a time lapse that depends on the number N of particles considered as $N^{1.7}$ after which the system eventually relaxes to equilibrium. This intermediate regime is called a QSS [9,10].

Let us now introduce the Vlasov equation describing the evolution of the distribution function $f(\theta, p)$ in the HMF model and valid in the thermodynamic limit [26,34]:

$$\begin{aligned} \frac{\partial f}{\partial t} + p \frac{\partial f}{\partial \theta} - \frac{dV[f]}{d\theta} \frac{\partial f}{\partial p} &= 0, \\ V[f](\theta) &= 1 - m_x[f] \cos \theta - m_y[f] \sin \theta, \\ m_x[f] &= \int d\theta dp f \cos \theta, \\ m_y[f] &= \int d\theta dp f \sin \theta, \end{aligned} \quad (3)$$

where θ is the periodic spatial coordinate, p is the momentum, and V is the potential, depending self-consistently on f . The

time evolution of Eqs. (3) conserves the energy U :

$$U[f](t) = \int d\theta dp f(\theta, p; t) \times \left[\frac{p^2}{2} + \frac{1}{2}(1 - m_x[f] \cos \theta - m_y[f] \sin \theta) \right], \quad (4)$$

the normalization

$$\int d\theta dp f(\theta, p; t) = 1,$$

and the total momentum

$$\int d\theta dp f(\theta, p; t) p.$$

In order to solve numerically Eqs. (3), we use the semi-Lagrangian method (see Ref. [35] or [36] for an application to the HMF model) with cubic spline interpolation. This method has been implemented in the code `vmf90` [37] used in Ref. [36] and in the present study. Although numerical limitations come into play [38], Vlasov simulations have proven useful to study the HMF model in the thermodynamic limit [34]. The semi-Lagrangian method displays a relatively small amount of numerical dissipation and thus fits adequately the purpose of computing the perimeter of the fluid.

Lynden-Bell's (LB) theory has proven so far successful for the HMF model [16,17] and the free-electron laser [10] and partly for the self-gravitating sheet model [11,25]. In particular, the phase diagram in the HMF model has been discussed in the framework of the LB theory by Staniscia *et al.*, who used the level of the distribution function f_0 for waterbag initial conditions, instead of the initial value of the magnetization m as the thermodynamical parameter that enters Lynden-Bell's theory, and evidenced a phase reentrance phenomenon that was not observed in previous studies [41]. An additional point of view on the core-halo structure that is found in the HMF model has been provided by Pakter and Levin [40], who introduced an ad hoc dynamical reduction as well as an ansatz on the distribution function f to find the stationary value for m_x and the corresponding f , respectively. In this way, these authors found a transition from $m_x > 0$ to $m_x = 0$ and an agreement for the position and velocity marginals of the distribution function in the inhomogeneous regimes [40].

As a matter of fact, the effectiveness of Lynden-Bell's theory to describe the HMF model has been an important confirmation of the adequateness of the Vlasov equation to understand QSS. It has been recently shown that Lynden-Bell's theory captures fundamental properties of the Vlasov dynamics and that phase-space *stirring* already provides a fair amount of evolution. The authors of Ref. [39] obtain good comparison between Lynden-Bell's theory and a model with no interaction at all between particles. The same authors propose an exact solution to the mean-field equilibria in the Vlasov equation, fully demonstrating how stirring allows the dynamics to reach steady states in Vlasov dynamics [8]. Stirring is however insufficient to obtain the better agreement found in the HMF model when using LB's theory. To complete the dynamical picture, another relaxation mechanism is needed.

III. EVOLUTION OF THE PERIMETER OF THE FLUID

In the context of 2D fluid dynamics, experimental results can be obtained by direct visual inspection. In the kinetic context, the distribution function (DF) lies in phase space (θ, p) . The technique that we propose is reminiscent of methods used in fluid dynamics. To analyze the complex behavior of the DF, we track its boundary in the same way as we would track a dyed region in a fluid. Instead of a dye, phase space is filled with a step profile of value f_0 . Inside the step, $f = f_0$, while outside of the step $f = 0$. An example of such step profiles is known as the waterbag (WB) initial condition. The WB initial condition possesses the following advantages: a simple formulation of LB's theory, a nice interpretation in terms of a dye in phase space, and a very widespread use in the literature.

The perimeter P_f of the DF f is the length of the interface between the $f = f_0$ and 0 regions of phase space; it is similar to the *intermaterial area per unit volume* defined in Ref. [42]. P_f provides a direct measure of the deformation of the DF.

The WB is defined by a width of $2\Delta\theta$ and $2\Delta p$ in the two dimensions of phase space. The initial perimeter P_f of this “fluid” is $4(\Delta\theta + \Delta p)$. The preservation of phase-space volume in Vlasov dynamics implies that the area of the fluid remains constant.

In the simple case of free streaming, it is easy to compute the time evolution of P_f :

$$P_f(t) = 4\Delta\theta + 4\Delta p\sqrt{1+t^2}, \quad (5)$$

which is seen to be asymptotically linear in time. This linear behavior is expected to hold in the case of regular dynamics, as in the case of integrable systems.

In more complex situations, we expect a deformation of the contour of the fluid, similar to what happens in fluid dynamics [42]. Indeed, 2D flows submitted to parametric forcing exhibit chaotic behavior, and analogies between Vlasov dynamics and 2D Euler equations are common [43]. If neighboring fluid elements experience an exponential separation of their

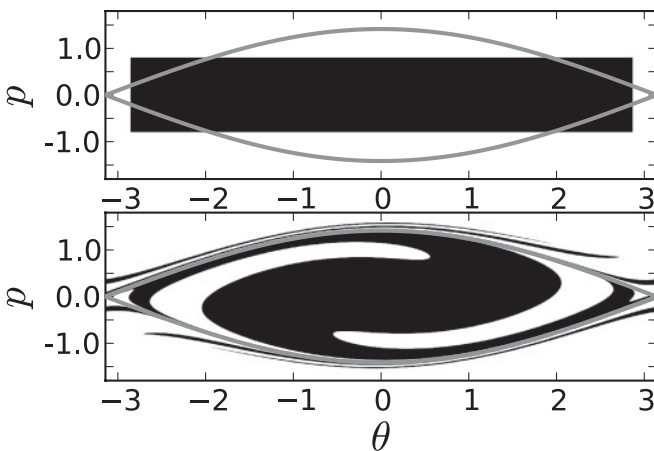


FIG. 1. Vlasov simulation for a noninteracting set of pendula. The top panel displays the waterbag initial condition, parametrized by $\Delta\theta = 2.85$ and $\Delta p = 0.79$. The bottom panel displays only the contour at time $t = 10$. The filamentary structure is caused, in this system, only by the differential rotation in phase space, i.e., phase-space *stirring*.

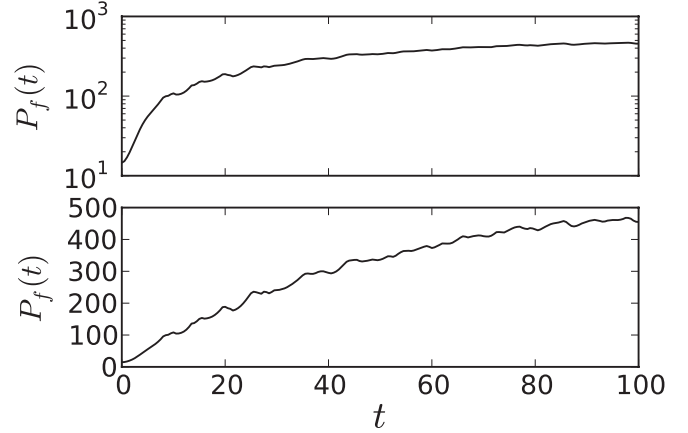


FIG. 2. Perimeter of the fluid as a function of time for the simulation shown in Fig. 1. The top panel uses a logarithmic scale on the y axis and the bottom panel uses a linear scale for the y axis.

positions, we expect that the perimeter is dominated by this contribution so that

$$P_f(t) \propto e^{\lambda t}, \quad (6)$$

where λ is a positive real number. After the stretching mechanism has taken place, the fluid folds onto itself to accommodate for the increasing perimeter at a fixed area. In fluid dynamics, the obtention of an optimal mixing, via stretching and folding of the fluid, is an ongoing topic of interest [42,44].

The perimeter is computed numerically with the help of the routine CONREC [45]. This routine, initially used to display contour lines on a computer display, has been modified in order to compute the length of this contour and has been implemented within the Vlasov simulation program used in Ref. [36], a modification that is necessary in order to avoid storing all time steps of the DF for postprocessing. Equation (5) is checked to give a perfect match with the simulation for $m = 0$ (data are not shown). A check of our conjecture for noninteracting systems is tested for a pendulum [a system similar to Eqs. (3) but in which the magnetization \mathbf{m} is set to a constant value in the equations of motion]. Figure 1 displays the evolution of the DF, and Fig. 2 displays the evolution of $P_f(t)$ for the same simulation.

Table I lists the numerical parameters for the Vlasov simulations. All initial conditions are run with all these parameters, allowing us to monitor the convergence of the physical quantities as a function of the number of grid points.

TABLE I. Numerical parameters for the Vlasov simulations.

	N_θ	N_p	Δt
0k5	512	512	0.1
1k	1024	1024	0.1
2k	2048	2048	0.1
4k	4096	4096	0.1
8k	8192	8192	0.1
8kb	8192	16384	0.1

TABLE II. Parameters for the waterbag initial condition of runs f , i , and j .

Run	U	m_0
f	0.60	0.20
i	0.69	0.20
j	0.565	0.50

IV. STRETCHING AND FOLDING IN PHASE SPACE

The present section focuses on the interacting HMF model. The variations of the self-consistent field \mathbf{m} cause a complex evolution of the initial waterbag that we consider in several test cases. The first case (run f in Table II) leads to a magnetized state and has the property that m_x keeps its sign in the course of time. Also, a significant amount of mass remains enclosed inside the separatrix at all times, meaning that it is not subject to alternating stretching motion but only to a stirring motion that is reminiscent of the noninteracting situation. A variation on run f is the run j , that also leads to a magnetized regime and possesses a similar structure in phase space. m_0 for run j is however equal to the predicted value of m in the QSS regime by Lynden-Bell’s theory, and we expect a smaller amount of stretching and folding because the variations of m are smaller. The second case (run i in Table II) refers to the peculiar value $U = 0.69$, with $m_0 = 0.20$, which is known to possess counter-rotating resonances. m_x then experiences changes of sign that imply elliptic-hyperbolic bifurcations [43], which we discuss further in Sec. IV B.

The organization of phase space is similar to that of a pendulum at every given time. The simplest situation is when $m_y = 0$ at all times with small variations of m_x around a finite average value. The system is then close to a set of pendula, although small oscillations of m_x are sufficient to induce stretching and folding. In the presence of stronger oscillations of m_x , the observed phenomenon of stretching and folding is increased. The oscillations of the separatrix, which drive the stretching and folding, are indeed linked to those of m_x . The region of phase space that is located under the separatrix at all times experiences deformations, but the organization of phase space is such that around the elliptic fixed point at (0,0) a part of the waterbag remains intact, recalling the “core-halo” phenomenon observed in self-gravitating systems [11,25].

In the counterpropagating resonances regime, first observed in Ref. [28], an example of hyperbolic-elliptic bifurcation is found. Such a behavior has been observed already in the single-wave model in Ref. [43]. The authors of the latter reference find that a succession of elliptic-hyperbolic bifurcation produces strongly chaotic Lagrangian trajectories and destroys dipolar structures, modifying the general behavior of the system. As it stands for the HMF model, two coherent counterpropagating clusters remain present in the system.

A. Variation of m_x at null m_y

We consider run f of Table II; in this situation, $m_y = 0$ at all times and m_x displays strong initial oscillations from $t = 0$ to $t \approx 100$, followed by smaller oscillations (see Fig. 3) around a finite value. The initial time lapse corresponds to violent

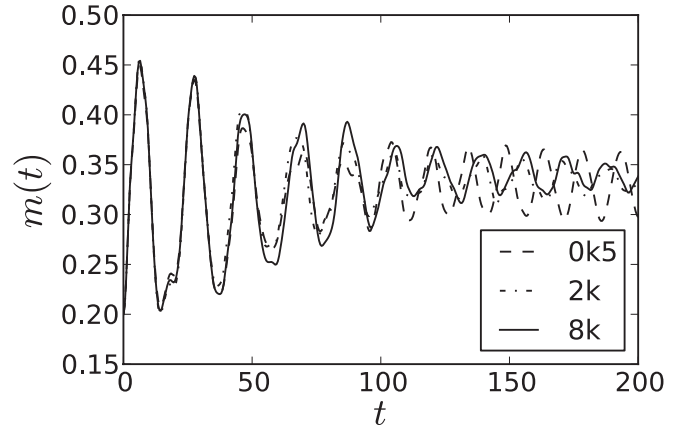


FIG. 3. Evolution of $m(t)$ as a function of the time t for run f of Table II for different numerical settings (see Table I). The initial behavior is very similar for all runs; later times display small phase and amplitude differences.

relaxation, during which we are interested in the behavior of the fluid. The initial stronger oscillations are typical of violent relaxation in self-gravitating systems, with the difference that the monitored quantity in these systems is the virial ratio [18]. The value of m , in the HMF model, is sufficient to fully follow macroscopic quantities.

Figure 3 displays $m(t)$ as a function of time, for run f and the parameters of Table I. Between $t = 0$ and $t \approx 50$, the curves superimpose well. Up to $t \approx 100$, qualitative agreement is still valid. We may already conclude that the amplitude of the oscillations decays, a key point in the theory of violent relaxation. However, the amplitude of the oscillations in $m(t)$ behaves in a different manner than that found in Ref. [36], where increasing the number of grid points enhances sustained oscillations. Here, increasing the number of grid points does not lead to a monotonous increase in the amplitude of the oscillations. We can quantify this behavior by taking the standard deviation of the time series $m(t)$, taken here between $t = 100$ and 200. The results are given in Table III. The standard deviation is observed to decrease from parameters “0k5” to “4k” and to increase afterward. This can be understood by the presence of two competing reasons for the damping. On the one hand, a low number of grid points increases the phenomenon of numerical dissipation (as found in Ref. [36]). On the other hand, a high number of grid points enables the description of complex dynamics in phase space such as stretching, folding, as well as the recurrence of coherent behavior, leading to moderate persistent oscillations of $m(t)$ as observed in the conditions of Fig. 3 with a fine enough resolution.

A general view of phase space is given in Fig. 4. The phase-space structure is as follows: there is an elliptic fixed point at

TABLE III. Standard deviations of $m(t)$ for run f with different parameters. $m(t)$ is taken between $t = 100$ and 200.

0k5	1k	2k	4k	8k	8kb
$2.5 \cdot 10^{-2}$	$1.7 \cdot 10^{-2}$	$1.3 \cdot 10^{-2}$	$1.1 \cdot 10^{-2}$	$1.5 \cdot 10^{-2}$	$1.6 \cdot 10^{-2}$

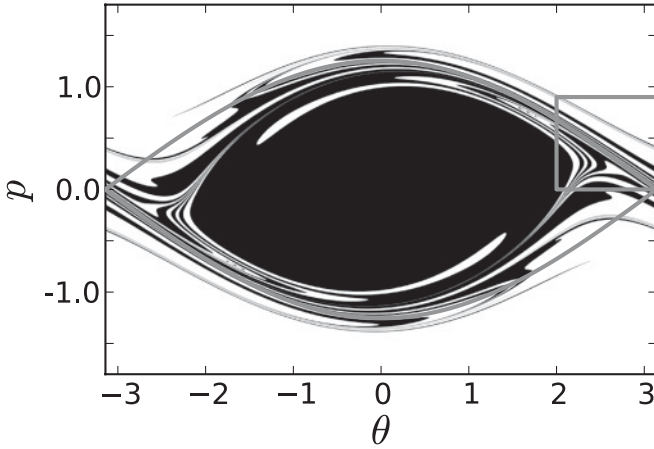


FIG. 4. Phase space for run f at time $t = 25$, with the setting “8k.” The contour is displayed, the region in black corresponds to $f = f_0$, and the region in white corresponds to $f = 0$. The instantaneous separatrix is drawn in gray and three separate regions are visible: well inside the separatrix, around the separatrix, and well above the separatrix. The filamentary structure is the result of the self-consistent evolution of the system. The box indicates the zoomed region of Fig. 6.

$(\theta, p) = (0, 0)$ and a hyperbolic fixed point at $(\theta, p) = (\pm\pi, 0)$. A separatrix joins the two hyperbolic points, but its height is variable as the magnetization evolves in time. This time dependence allows one to consider the HMF model as a time-dependent pendulum, keeping in mind that in the HMF model the particles generate self-consistently the value of \mathbf{m} . Three different behaviors are found, depending on the energy with respect to the separatrix, consistent with the findings of the forced pendulum [29]: (1) Below the separatrix energy, the so-called trapped particles remain close to the elliptical point and perform an oscillatory motion; (2) above the separatrix, particles cross space with a velocity of constant sign; and (3) at energies near the separatrix, particles experience a very complex behavior, known as separatrix crossing. The

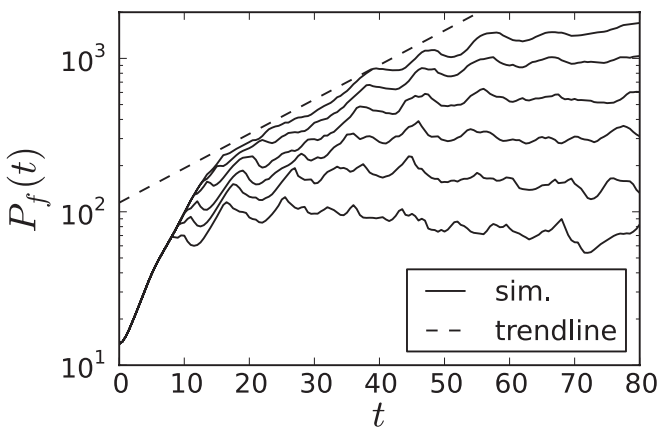


FIG. 5. The perimeter $P_f(t)$ for run f , for several configurations of Table I. The initial behavior is an exponential increase of P_f as a function of time (notice the logarithmic scale for the y axis), followed by a saturation due to a numerical limitation. It is observed that increasing the number of grid points increases the saturation level.

oscillations of the separatrix will cause fluid elements to experience stretching and folding.

Figure 5 displays $P_f(t)$ for the parameters from Table I. The initial behavior of $P_f(t)$ is exponential (notice the logarithmic scale of P_f in Fig. 5), showing that part of the perimeter is experiencing an early exponential separation. Thereafter, the perimeter goes up and down depending on the resolution used in the simulation. If the resolution is too low, the perimeter culminates and decreases due to the inability of the numerical procedure to resolve structures that are finer than the numerical grid. If the number of grid points is increased, the problem is delayed farther and farther. With our finer resolution, the perimeter is observed in Fig. 5 to saturate on the time interval considered, after a moderate growth shown with the dashed line.

A general comment is that the stretching rate λ of the perimeter differs from a Lyapunov exponent in several respects. A study of the Lyapunov exponent for test particles submitted to the force field of a Vlasov-Poisson plasma has been performed in a stationary regime and reveals interesting similarities in the organization of phase space around the separatrix [46]. However, the method introduced in the present work automatically tracks the boundary of the distribution function and follows the time evolution of its perimeter. Since the perimeter is associated with a certain distribution function, its stretching rate only characterizes the phase-space regions at the boundary of the distribution function, which depends in general on the choice of the initial distribution function. Moreover, depending on the conditions, the perimeter may undergo an early regime of exponential growth that does not go on, so that the stretching rate may not be defined in the long-time limit contrary to Lyapunov exponents. Nevertheless, the concept of the Lyapunov exponent characterizing chaotic dynamics is useful to interpret the present stretching rate. In Fig. 5, the early exponential increases observed for P_f can be understood in terms of the phase-space dynamics of the pendulum periodically forced by the large early oscillations of the mean field seen in Fig. 3. Indeed, the periodically forced pendulum is known to be chaotic, which can induce the stretching of phase-space domains leading to a positive Lyapunov exponent. Therefore, the perimeter can undergo an exponential growth as long as this induced stretching goes on. However, as time increases, the oscillations of the mean field become of lower amplitudes as observed in Fig. 3, which reduces the extension of the chaotic zones in the phase space of the periodically forced pendulum and tends to decelerate the growth of P_f as seen in Fig. 5. This decrease is expected to hold under the assumption of mixing, but the numerical limitations explained earlier in this section affect the behavior of P_f at earlier times as the numerical resolution becomes lower. We point out that the self-consistent setting used in the present work is needed in order to study the phenomenon of violent relaxation itself, in contrast to the situation of the periodically forced pendulum. The dynamical evolution from an initial condition to a QSS is indeed specific to the problem of violent relaxation.

Finally, to illustrate the behavior at small scales, we display in Fig. 6 a zoom of Fig. 4 at a later time. The stretching and folding structures are clearly apparent.

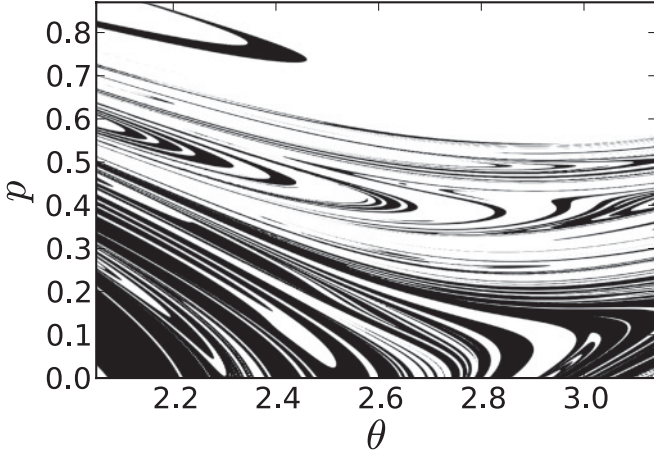


FIG. 6. Zoom on Fig. 4 at a later time $t = 100$. The complex evolution of the initial waterbag leads to a stretching and folding behavior. A very intricate sequence of $f = 0$ and f_0 regions can be observed.

B. Elliptic-hyperbolic bifurcation

The study of run i , leading to the counterpropagating resonances, displays an interesting bifurcation of the elliptic fixed point $(0,0)$. The nature of that point depends on the sign of m_x that is found to change during time evolution. The separatrices corresponding to the two situations of the elliptic-hyperbolic bifurcation are shown in Fig. 7.

The evolutions of m and m_x are displayed in Fig. 8 ($m_y = 0$ at all times). Fluid elements that are located in the alternating separatrix regions experience a strong amount of stretching and folding. This is confirmed in Fig. 9, where $P_f(t)$ is shown and compared to the result for run f . The improved mixing in run i should not however lead to premature conclusions about the relaxation of the systems on a macroscopic level. The counter propagating resonances are very stable and prevent the relaxation to complete equilibrium, in which the resonances are not predicted.

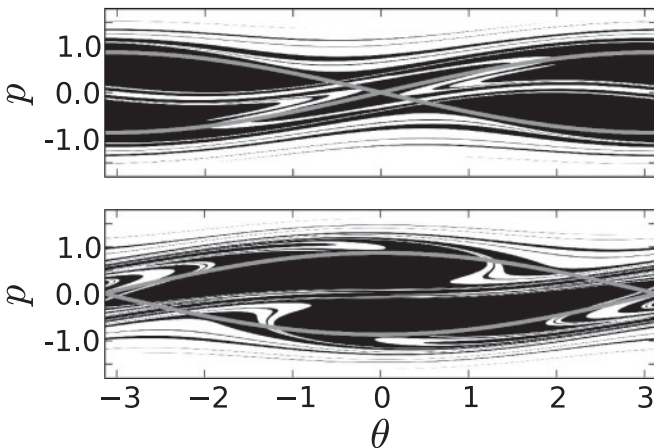


FIG. 7. Phase-space DF $f(\theta, p)$ for run i at time $t = 20$ and 25 (see Fig. 8). Two counterpropagating clusters are found that lead to sign changes in m_x . The top panel displays a separatrix for $m_x < 0$ and the bottom panel displays a separatrix for $m_x > 0$.

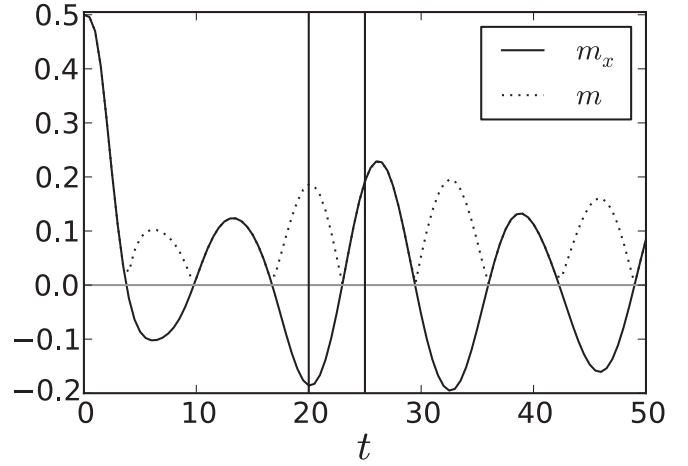


FIG. 8. m_x and m as a function of time for run i . The vertical lines indicate the times at which the snapshots of Fig. 7 are taken.

In order to link the phenomenon of stretching and folding to the amount of evolution from an initial condition to a QSS, run j provides an interesting comparison. The initial magnetization is $m_0 = 0.5$, and the magnetization predicted by Lynden-Bell’s theory is also $m_{QSS} = 0.5$. A large region of the initial waterbag will remain below the separatrix, and smaller oscillations than for run f are expected. A comparison between run f and run j for the numerical parameters 8kb is given in Fig. 9, confirming that the amount of stretching and folding needed for run j is well below that for run f .

V. MEAN-FIELD MAPS

In this section, we simplify the dynamics of the HMF model into discrete-time maps giving the mean-field approximation of symplectic coupled map systems [47] ruled by the periodically kicked Hamiltonian:

$$H = \sum_{i=1}^N \frac{p_i^2}{2} + \left[\sum_{i=1}^N U_0(x_i) + \frac{1}{2N} \sum_{i,j=1}^N U(x_i - x_j) \right] \times \sum_{n=-\infty}^{+\infty} \delta(t - n). \tag{7}$$

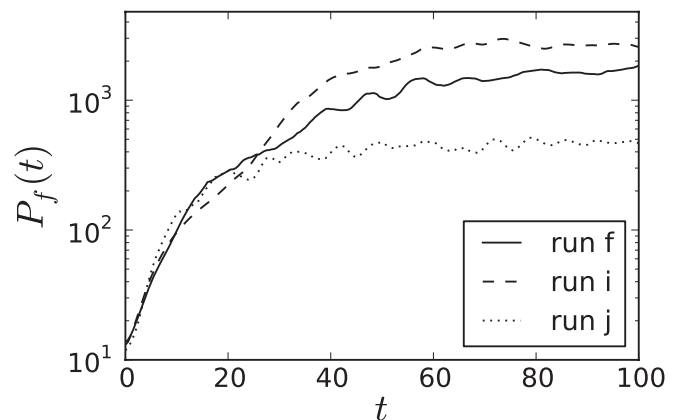


FIG. 9. The perimeter $P_f(t)$ for the runs f, i , and j of Table II. All runs are performed with the setting “8kb” of Table I.

In the mean-field approximation, the positions and momenta of the particles after each kick are mapped by the time evolution according to

$$\Phi \begin{cases} p_{n+1} = p_n - U'_0(x_n) - \int dx dp f(x, p) U'(x_n - x) \\ x_{n+1} = x_n + p_{n+1} \quad (\text{modulo } 1), \end{cases} \quad (8)$$

where n denotes the discrete time and $f(x, p)$ denotes the distribution function representing the ensemble of particles normalized by $\int f(x, p) dx dp = 1$. The map is area preserving so that the normalization condition is maintained during the time evolution. Here, we consider the interaction $U(x) = C [1 - \cos(2\pi x)] / (2\pi)$ and the external potentials: $U_0 = -Kx^2/2$, corresponding to Arnold's cat map [30,31], or $U_0 = A [\cos(2\pi x) - 1] / (2\pi)$, giving the standard map [32,33].

We suppose that the distribution function $f(x, p)$ is uniform in a phase-space domain D_n . This domain evolves in time under the mean-field mapping, $D_n = \Phi^n(D_0)$, and its area is preserved: $\text{Area}(D_n) = \text{Area}(D_0)$. The problem is now to determine the time evolution of the perimeter of the domain D_n . In this regard, we notice that the domain D_n has the same perimeter whether it is defined on the cylindrical phase space $\{0 \leq x < 1, -\infty < p < +\infty\}$ or in the whole plane $\{-\infty < x < +\infty, -\infty < p < +\infty\}$, because the mean field is the same in both cases. Accordingly, the perimeter can also be calculated without imposing periodicity in the position x , which provides a numerical advantage.

A. Mean-field cat map

Here, the map takes the following form:

$$\begin{cases} p_{n+1} = p_n + Kx_n - m_x[f] \sin(2\pi x_n) + m_y[f] \cos(2\pi x_n) \\ x_{n+1} = x_n + p_{n+1} \quad (\text{modulo } 1), \end{cases} \quad (9)$$

with the mean field equation

$$\mathbf{m}[f] = m_x[f] + i m_y[f] = C \int dx dp f(x, p) e^{i2\pi x}. \quad (10)$$

The initial distribution function $f(x, p)$ is taken to be uniform in a circle of radius $\frac{1}{4}$ centered on the point $x = p = \frac{1}{2}$ of the unit square, which defines the initial domain D_0 . After n iterations, the distribution function is still uniform but in a domain D_n resulting from the time evolution of the map Eq. (9).

If the coupling parameter vanishes, $C = 0$, the mean field has no effect on the dynamics and the map reduces to Arnold's cat map, which is known to be fully chaotic if the parameter K is a positive integer [30,31]. We notice that the hyperbolic character of the map persists as long as the coupling parameter C is small enough that $K \gg 2\pi |\mathbf{m}|$. Under this condition, we may expect that the hyperbolic character of the map will tend to stretch the domain D_n into a filamentary phase-space structure, which produces an effective uniform distribution over the unit interval x such that the mean field Eq. (10) tends to vanish as $n \rightarrow \infty$. For the same reason, the perimeter of the domain D_n grows exponentially in time at a rate close to the Lyapunov exponent of the Arnold cat map. This is indeed observed in Fig. 10, which depicts the perimeter of the domain D_n versus the number n of iterations for the parameter values

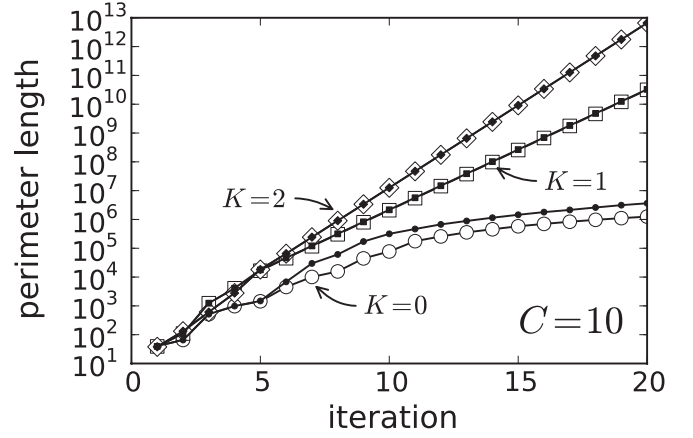


FIG. 10. The perimeter $P_f(t)$ for the mean-field cat map with $K = 0, 1, 2$ and $C = 10$. The calculations are performed with 1×10^6 (empty symbols) and 4×10^6 (full symbols) points to represent the boundary and the bulk of the domain where the distribution function is uniform.

$C = 10$ and $K = 0, 1, 2$. The computation is performed for two approximations in which the boundary of the domain D_n and its interior are discretized into 1×10^6 and 4×10^6 points. In the hyperbolic regime for $K = 1$ and 2 , the growth of the perimeter is exponential. However, in the absence of chaos for $K = 0$, the perimeter no longer increases exponentially and the computation is sensitive to the discretization. The fact is that, for the value $C = 10$ of the coupling parameter, the mean field vanishes so that the mean field alone cannot induce an exponential stretching of the perimeter in this case.

B. Mean-field standard map

Now, we consider the mean-field standard map defined on the unit square as

$$\begin{cases} p_{n+1} = p_n + (A - m_x[f]) \sin(2\pi x_n) + m_y[f] \cos(2\pi x_n) \\ x_{n+1} = x_n + p_{n+1} \quad (\text{modulo } 1), \end{cases} \quad (11)$$

with the same mean field as in Eq. (10). Here, the single-particle potential as well as that induced by the mean field have a similar trigonometric form so that the mean field m_x appears to have an effect comparable to that of the constant parameter A of the standard map (in the case where $m_y = 0$) [32,33]. The initial distribution function $f(x, p)$ is the same as in the previous subsection.

Figure 11 shows the growth of the perimeter of the domain D_n as a function of the discrete time n for the parameter values $C = 1$ and $A = 0, 1, 2$. As before, the boundary and the bulk of the domain D_n are discretized into 1×10^6 and 4×10^6 points. The early growth of the perimeter until about $n = 6$ iterations is well approximated by these discretizations for $A = 1, 2$ and until about $n = 15$ iterations for $A = 0$. Thereafter, both approximations deviate, showing the sensitivity of the calculation to the discretization of the domain D_n and the distribution function $f(x, p)$ into points. Nevertheless, the early growth appears to be exponential for $A = 0, 1, 2$.

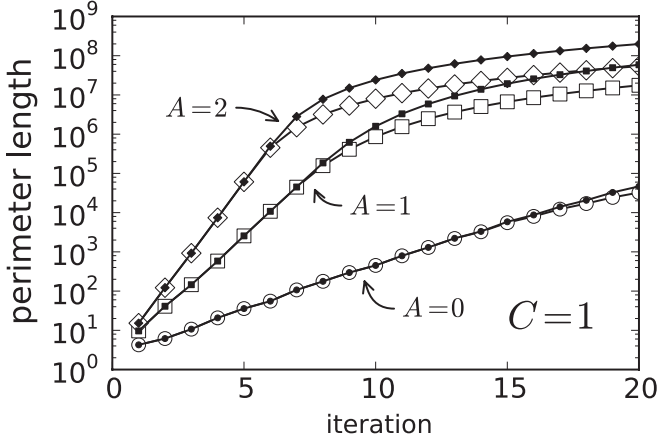


FIG. 11. The perimeter $P_f(t)$ for the mean-field standard map with $K = 0, 1, 2$ and $C = 1$. The calculations are performed with 1×10^6 (empty symbols) and 4×10^6 (full symbols) points to represent the boundary and the bulk of the domain where the distribution function is uniform.

For $A = 1, 2$, the exponential increase of the perimeter can be explained by the global chaoticity of the standard map for $A > A_c \simeq 0.15$ [32,33]. Indeed, the standard map is stretching domains at a rate equal to the Lyapunov exponent $\lambda \simeq \ln(\pi A)$, which is positive for $A = 1, 2$. At each iteration, the perimeter of the domain D_n is stretched by a factor $\exp(\lambda) > 1$ for every point in the chaotic zones of the map. The domain D_n thus develops a filamentary phase-space structure uniformly distributed over the unit square so that the mean field Eq. (10) tends to vanish and the mean-field standard map Eq. (11) behaves on long time as the single-particle standard map with $A = 1, 2$ and $\mathbf{m} = 0$. Accordingly, the exponential growth of the perimeter of the domain D_n could go on as the discrete time n increases.

In contrast, for $A = 0$, the dynamics is entirely determined by the mean field Eq. (10). It turns out that the mean field vanishes for $C > C_t$ with $C_t \simeq 2$ but is nonvanishing for $0 < C < C_t$ by a phenomenon analogous to the one happening in the HMF model. For $C = 1$, the mean field fluctuates around the mean value $m_x \simeq -0.21$ with $m_y = 0$. This explains the early exponential growth of the perimeter observed in Fig. 11 for $A = 0$ and $C = 1$. Indeed, if we suppose that the mean field remains essentially constant, the Vlasov dynamics would be equivalent to that of the simple standard map for $A = -m_x \simeq 0.21$. In this case, the early growth rate would be about $\lambda \simeq 0.44$, which is close to the value $\lambda \simeq 0.48$ of the mean-field dynamics with $A = 0$ and $C = 1$ shown in Fig. 11.

These results confirm that the stretching of the perimeter by the Vlasov dynamics is controlled by the local hyperbolicity of the effective single-particle phase-space dynamics induced by the current value of the mean field.

VI. CONCLUSION

Measuring the degree of mixing in kinetic theory is undoubtedly a considerable challenge. Nevertheless, in order to assess the evolution of a given system, we here propose

a quantitative tool by drawing an analogy with the mixing of dyed regions in fluid mechanics. In this picture, the effectiveness of the mixing can be measured by the growth of the perimeter of dyed fluids in phase space.

In both the Hamiltonian mean-field model and the mean-field cat and standard maps, our numerical simulations report an exponential growth of the perimeter, a sign that exponential stretching occurs at least locally on the contour of the dyed fluid. The fluid in phase space displays folding and stretching structures that are absent from similar noninteracting and non-chaotic systems. This mechanism is an appropriate candidate to explain how violent relaxation can take place: through mixing in phase space, even though this mixing is limited to certain regions of phase space.

The complex intertwining of $f = 0$ and f_0 regions in phase space confirms that a coarse-grained theory should be able to provide a good description of the fluid after mixing has taken place. The existence of an infinite number of conserved quantities in the Vlasov equation forbids the increase of entropic functionals, which implies that coarse graining is needed in order to describe the evolution toward stationary states or quasistationary states (QSS). In the light of our findings about the mechanism leading to such QSS, violent relaxation can be understood from a Vlasovian point of view, in which the deformation of the initial condition allows the system to reach a QSS. This deformation takes place at constant phase-space volume but with a perimeter that increases exponentially during some lapses of the time evolution. The increase in the perimeter is made possible through successive stretching and folding of the fluid. Subsequently, finite N effects may come into play, but they are of a different type and are not discussed herein.

We notice that the results of the present article are in agreement with the understanding of phenomena related to violent relaxation, for instance the separation of phase space into different regions [48] that leads to the formation of a core and a halo. Applying our method to more common systems, such as the self-gravitating sheet model, is expected to reveal a similar behavior and would prove interesting to complete the existing body of literature.

As known in the literature, the presence of self-consistent resonances may organize phase space in a way that prevents the statistical prediction of stationary regimes. Indeed, these resonances imply that the energy distribution function is nonmonotonous, in contrast to the predictions of Lynden-Bell’s theory or Boltzmann-Gibbs equilibrium. The self-consistent resonances are often at the origin of the so-called “dynamical effects” that prevent a system from reaching a QSS or thermodynamical equilibrium.

Finally, let us recall that, in the perspective given in the present paper, the phase-space exponential separation leading to mixing has similarities to what happens in chaotic dynamics, although notable differences exist such that the dependence on the initial distribution function as well as the time dependence of the stretching rate. A possible way to tighten both aspects is to use test particles that feel the time-dependent magnetization generated by a Vlasov simulation. It is possible to push this method further by the use of a Poincaré map on these test particles, providing one with the tools of iterative mapping, which are of common use in nonlinear dynamics.

ACKNOWLEDGMENTS

This research is financially supported by the Belgian Federal Government (Interuniversity Attraction Pole project

“NOSY” P6/02, “Nonlinear systems, stochastic processes, and statistical mechanics”). P.d.B. thanks R. Kapral for support.

-
- [1] T. Dauxois, S. Ruffo, E. Arimondo, and M. Wilkens, *Dynamics and Thermodynamics of Systems with Long Range Interactions*, Vol. 602 of Lecture Notes in Physics (Springer-Verlag, New York, 2002).
- [2] A. Campa, A. Giansanti, G. Morigi, and F. Sylos Labini, *Dynamics and Thermodynamics of Systems with Long Range Interactions: Theory and Experiments, Assisi, Italy 4–8 July 2007*, Vol. 970 of AIP Conference Proceedings (American Institute of Physics, Woodbury, 2008).
- [3] A. Campa, T. Dauxois, and S. Ruffo, *Phys. Rep.* **480**, 57 (2009).
- [4] Y. Y. Yamaguchi, J. Barré, F. Bouchet, T. Dauxois, and S. Ruffo, *Physica A* **337**, 36 (2004).
- [5] F. Bouchet and T. Dauxois, *Phys. Rev. E* **72**, 045103(R) (2005).
- [6] K. Jain, F. Bouchet, and D. Mukamel, *J. Stat. Mech.* (2007) P11008.
- [7] E. Caglioti and F. Rousset, *Arch. Rational Mech. Anal.* **190**, 517 (2008).
- [8] P. de Buyl, D. Mukamel, and S. Ruffo, e-print [arXiv:1012.2594](https://arxiv.org/abs/1012.2594) (2010).
- [9] V. Latora, A. Rapisarda, and S. Ruffo, *Phys. Rev. Lett.* **83**, 2104 (1999).
- [10] J. Barré, T. Dauxois, G. De Ninno, D. Fanelli, and S. Ruffo, *Phys. Rev. E* **69**, 045501 (2004).
- [11] Y. Y. Yamaguchi, *Phys. Rev. E* **78**, 041114 (2008).
- [12] R. Bachelard, T. Manos, P. de Buyl, F. Staniscia, F. S. Cataliotti, G. D. Ninno, D. Fanelli, and N. Piovella, *J. Stat. Mech.* (2010) P06009.
- [13] M. Hénon, *Annales d’Astrophysique* **27**, 83 (1964).
- [14] M. Lecar, Proceedings of the International Astronomical Union, IAU Symposium **25**, 46 (1966).
- [15] D. Lynden-Bell, *Mon. Not. R. Astron. Soc.* **136**, 101 (1967).
- [16] A. Antoniazzi, D. Fanelli, J. Barré, P.-H. Chavanis, T. Dauxois, and S. Ruffo, *Phys. Rev. E* **75**, 011112 (2007).
- [17] A. Antoniazzi, D. Fanelli, S. Ruffo, and Y. Y. Yamaguchi, *Phys. Rev. Lett.* **99**, 040601 (2007).
- [18] F. Hohl, NASA Technical Report No. R-289 (1968) (unpublished).
- [19] M. Luwel and G. Severne, *Astron. Astrophys.* **152**, 305 (1985).
- [20] P. Mineau, M. R. Feix, and J. L. Rouet, *Astron. Astrophys.* **228**, 344 (1990).
- [21] Y. Funato, J. Makino, and T. Ebisuzaki, *Publ. Astron. Soc. Jpn.* **44**, 613 (1992).
- [22] Y. Levin, R. Pakter, and T. N. Teles, *Phys. Rev. Lett.* **100**, 040604 (2008).
- [23] T. Teles, Y. Levin, R. Pakter, and F. Rizzato, *J. Stat. Mech.* (2010) P05007.
- [24] M. Joyce and T. Worrakitpoonpon, *J. Stat. Mech.* (2010) P10012.
- [25] M. Joyce and T. Worrakitpoonpon, *Phys. Rev. E* **84**, 011139 (2011).
- [26] R. Balescu, *Statistical Dynamics—Matter out of Equilibrium* (Imperial College Press, London, 1997).
- [27] T. O’Neil and F. Coroniti, *Rev. Mod. Phys.* **71**, S404 (1999).
- [28] M. Antoni and S. Ruffo, *Phys. Rev. E* **52**, 2361 (1995).
- [29] Y. Elskens and D. F. Escande, *Nonlinearity* **4**, 615 (1991).
- [30] I. Percival and F. Vivaldi, *Physica D* **27**, 373 (1987).
- [31] M. M. Sano, *Phys. Rev. E* **66**, 046211 (2002).
- [32] B. V. Chirikov, *Phys. Rep.* **52**, 265 (1979).
- [33] A. J. Lichtenberg and M. A. Lieberman, *Regular and Stochastic Motion* (Springer, New York, 1983).
- [34] A. Antoniazzi, F. Califano, D. Fanelli, and S. Ruffo, *Phys. Rev. Lett.* **98**, 150602 (2007).
- [35] E. Sonnendrucker, J. Roche, P. Bertrand, and A. Ghizzo, *J. Comp. Phys.* **149**, 201 (1999).
- [36] P. de Buyl, *Commun. Nonlinear Sci. Numer. Simulat.* **15**, 2133 (2010).
- [37] P. de Buyl (unpublished).
- [38] F. Califano, L. Galeotti, and A. Mangeney, *Phys. Plasmas* **13**, 082102 (2006).
- [39] P. de Buyl, D. Mukamel, and S. Ruffo, *Philos. Trans. R. Soc. London A* **369**, 439 (2011).
- [40] R. Pakter and Y. Levin, *Phys. Rev. Lett.* **106**, 200603 (2011).
- [41] F. Staniscia, P. H. Chavanis, G. De Ninno, and D. Fanelli, *Phys. Rev. E* **80**, 021138 (2009).
- [42] J. M. Ottino, *The Kinematics of Mixing: Stretching, Chaos and Transport* (Cambridge University Press, Cambridge, 1989).
- [43] D. del Castillo-Negrete and M.-C. Firpo, *Chaos* **12**, 496 (2002).
- [44] S. Wiggins and J. M. Ottino, *Philos. Trans. R. Soc. London A* **362**, 937 (2004).
- [45] P. Bourke, *Byte Magazine* **12**, 143 (1987).
- [46] F. Valentini, V. Carbone, P. Veltri, and A. Mangeney, *Phys. Rev. E* **71**, 017402 (2005).
- [47] T. Konishi and K. Kaneko, *J. Phys. A: Math. Gen.* **25**, 6283 (1992).
- [48] T. Yamashiro, N. Gouda, and M. Sakagami, *Prog. Theor. Phys.* **88**, 269 (1992).